PAPER VI

# Modeling of the time-averaged gas–solid drag force in a fluidized bed based on results from transient 2D Eulerian–Eulerian simulations

Powder Technology 261 (2014b) 257–271.

Powder Technology 261 (2014) 257–271

Contents lists available at ScienceDirect

Powder Technology

journal homepage: www.elsevier.com/locate/powtec

# Modeling of the time-averaged gas–solid drag force in a fluidized bed based on results from transient 2D Eulerian–Eulerian simulations

Sirpa Kallio *, Juho Peltola, Timo Niemi

*VTT Technical Research Centre of Finland, P.O. Box 1000, FI-02044 VTT, Finland*

ARTICLE INFO

*Article history:*
Received 11 February 2014
Received in revised form 4 April 2014
Accepted 9 April 2014
Available online 18 April 2014

*Keywords:*
Drag force
Circulating fluidized bed
Time-averaging
Computational fluid dynamics
Empirical modeling

ABSTRACT

In the present paper, the possibilities to cover all fluidization states by a single drag law in steady-state CFD multiphase flow modeling are evaluated. The time-averaged drag force is expressed as the product of the drag force calculated from the traditional drag laws for homogeneous conditions, and a correction function. Closure correlations for the correction function are developed by nonlinear regression modeling based on data collected from 69 transient 2D simulations of bubbling, turbulent and circulating fluidized beds. The correlations are given as functions of eight variables: the solid volume fraction, the distance from the nearest wall, the height above the air distributor, the slip velocity between the phases, the gas velocity, the particle size, the solid density and the gas viscosity. The results indicate that covering all fluidized bed conditions in a single drag correlation is feasible, although fully satisfactory results were not obtained for the surface and freeboard regions of a bubbling fluidized bed (BFB) with correlations that were acceptable in circulating fluidized bed (CFB) conditions. A correlation that covers the whole range of fluidized states is complicated and thus the modeling task could be divided into development of separate correlations for different regions that could be combined into a single correlation by means of blending functions. The validity of this approach was demonstrated by developing a separate correlation for the dilute conditions above a height of 1.5 m in CFB risers. Results show that the accuracy of the predictions significantly improved in dilute CFB conditions where a much simpler correlation with six input variables could be used. The modeling approach is a good starting point for the development of a general drag law for CFD simulations of fluidized beds.



## 1. Introduction

Steady-state simulation is an attractive alternative for simulations of industrial-scale circulating fluidized bed (CFB) processes [1,2] since the tedious integration over a long time, as applied on transient simulation results, is generally avoided [1]. The clustering of particles in CFB gas–solid flows produces steep local gradients and structures in the solid volume fraction field. In transient simulations, these details have to either be resolved numerically, which requires a fine spatial and temporal resolution, or accounted for by means of closure laws that comprise the effects of the unresolved flow structures. In a steady-state simulation only the statistical properties of the fine structures need to be resolved and thus a coarser mesh suffices, allowing to shorten the simulation time. The equations for steady-state simulations can be derived by time-averaging the transient continuity and momentum equations. The temporal variations in the flow properties are modeled with closure relations that can be derived e.g. through analysis of time-averaged transient simulation results [1].

One of the largest terms in the time-averaged momentum equations is the gas–solid drag force [3]. Since a dense gas–solid flow is characterized by large fluctuations in flow properties, the drag models suitable for homogeneous conditions and used in transient simulations are not applicable in time-averaged modeling. Some attempts have been made to derive a closure for the time-averaged drag force (De Wilde et al. [4,5], Kallio et al. [6] based on Matsen [7]). Typically, the average force is expressed as a product of the drag force calculated from the traditional drag laws for homogeneous conditions (e.g. Wen and Yu [8] and Gidaspow [9] drag laws) and a correction function. In Kallio et al. [10], the parameters that could have significant effects on the correction function in CFB conditions were identified. The analysis was carried out by time-averaging results from 17 transient 2D simulations of CFB risers. The parameters that were shown to be important were the solid volume fraction, the distance from the nearest wall, the slip velocity between the phases, the particle size, the solid material density and the gas viscosity. Kallio et al. studied the qualitative effects of different variables one by one, thus not taking into account the possible combined effects of two or more variables. Still, some complicated joint effects of wall distance and slip velocity were observed. Similarly, the effects of material properties and solid concentration were shown to interact: the correction function values at a specific solid volume fraction

* Corresponding author. Tel.: +358 20 7224015.
*E-mail address:* sirpa.kallio@vtt.fi (S. Kallio).

http://dx.doi.org/10.1016/j.powtec.2014.04.045
0032-5910/

were significantly affected by changes in the material properties and these effects were different for different ranges of solid concentration. More data are needed if the data are to be used both for extending the models to all relevant conditions and for covering the combined effects of several parameters. To evaluate combined effects of different material properties, several combinations of material property values need to be included in the data. In the present work, data from new simulations are added to the data set of Kallio et al. [10] with the aim to cover a wider range of fluidization conditions. Like the previous study, the present investigation is limited to Geldart B particles [11].

By definition, the correction function for the time-averaged drag force has a value of unity in homogeneous flow conditions. In inhomogeneous conditions it deviates from unity and is typically reduced [10]. The inhomogeneity of a suspension does not necessarily depend only on the local flow properties and the distance from the walls, but may be affected by the formation and the transport of the flow structures, such as clusters, strands and voids. Thus there is the possibility that the efforts to derive a general drag correction function based on the local voidage, velocities and material properties may fail. The goal of the present study is thus to evaluate the possibilities to express a general drag closure law for the time-averaged momentum equation entirely on the basis of the local variables and location.

The results of Kallio et al. [10] indicate that it is not easy to a priori define the functional form of the required closure model. A solution to the problem, presented here, is a nonlinear regression model with a functional form adjusting to the observed behavior. Although the available amount of data is fairly limited, it is sufficient to demonstrate the potential of this modeling approach. In this work, data from 2D simulations are used as the basis for nonlinear empirical modeling of the drag force and the feasibility and the limitations of the approach are discussed. The parameters in the correlations developed in this work are not presented, since due to the 2D simplification and the limited amount of data they should only be considered as a proof of the concept. It would not be advisable to implement them in a CFD model in the present form.

## 2. Transient Eulerian–Eulerian 2D simulations

In the present work, transient Eulerian–Eulerian CFD simulations in different fluidization conditions are used as the basis for model development. The geometry in all the simulated cases is a simple, rectangular riser with straight walls. A gas inflow is introduced at the bottom and the gas and the solid phase exit the riser through the top edge of the simulated domain. Solids that leave the riser are fed back to the riser at a height of 0.6–0.7 m through a return channel. A schematic of the geometry is presented in Fig. 1. Most of the simulations in this work were carried out in a small geometry with a bed width of 0.4 m, but one fourth of the simulated fluidized beds were larger with widths ranging from 0.9 m to 6 m. A uniform gas inflow rate is applied in most simulations in CFB conditions while in the rest of the CFB simulations air flows in through nozzles, which are either described as separate openings located about 0.05 m from each other or by means of a function that defines the local gas velocity. At lower fluidization rates applied in BFB conditions air is in most simulations introduced through orifices placed about 0.05 m apart from each other to allow for more typical formation of bubbles.

In all the simulation cases a uniform mesh was used. Kallio et al. [10] observed that simulations with a mesh spacing of 12 mm gave nearly the same result for the correction coefficient for the time-averaged drag force as simulations in a finer mesh with 6 mm elements. Li et al. [12] showed that the required mesh resolution varies depending on the property that is studied. For some other properties a finer mesh could be necessary, but for the drag analysis a mesh spacing of 12 mm suffices. Thus to save computation effort, most of the runs presented in this work were carried out with 12-mm and 10-mm mesh resolutions. Kallio et al. [10] also concluded that the riser width, the solid

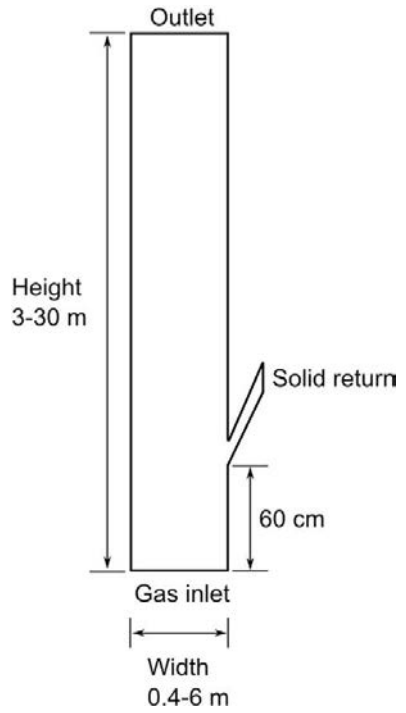


**Fig. 1.** Geometry in the transient simulations.

inventory and the fluidization velocity have no significant effects on the drag correction function in CFB conditions. However, in bubbling fluidized bed (BFB) conditions, the flow structure is very different and thus the fluidization velocity is likely to have an effect when the fluidization mode changes from BFB to CFB. The set of CFB simulations used in Kallio et al. [10] was therefore extended to cover a wider range of process conditions. The new set includes data also from turbulent fluidized bed (TFB) and bubbling fluidized bed conditions. Because of a wide particle size distribution and a reduced gas velocity at the bottom, the suspension density in the bottom region of an industrial CFB combustor is often relatively high, close to the densities found in turbulent and bubbling bed conditions. Thus a correlation for dense suspensions is required even when the correlation is applied on an industrial CFB process as the goal is to cover the whole riser section of the device.

Data from 69 simulations were included in the analysis. The analyzed cases are listed in Table 1. Although an even larger amount of data would be required in order to fully cover all the possible combinations of the values of the input variables, this data set was considered to be sufficient for the present study, whose aim is to verify the suitability of the proposed modeling approach. To derive a final correlation with higher accuracy, additional simulations in 3D and with a larger set of combinations of material property values should be included in the analysis.

The numerical simulations were carried out with the commercial code ANSYS Fluent v.14 [13] with the Eulerian–Eulerian multiphase approach based on the kinetic theory of granular flow (KTGF). In all the simulations, the solid phase is assumed to consist of monodispersed spherical particles. The multiphase flow equations along with the kinetic theory closure models are listed in Table 2. All the closure models used here are available in Fluent v.14.

The drag term was computed from the Gidaspow [9] drag model, which combines the Ergun [18] and Wen and Yu [8] drag laws. For the momentum equation, a second-order upwind convection scheme was

**Table 1**
Analyzed cases.

| Case | Type | $U_0$ (m/s) | $\mu_g$ (kg/ms) | $\rho_g$ (kg/m$^3$) | $\rho_s$ (kg/m$^3$) | $d_p$ (mm) | $\Delta x_{mesh}$ (mm) | $w$ (m) | $h$ (m) | $v_t$ (m/s) |
|---|---|---|---|---|---|---|---|---|---|---|
| 1 | u | 2.5 | 4.45E-05 | 0.3105 | 2480 | 0.2555 | 12.5 | 0.4 | 3 | 1.53 |
| 2 | f | 3.14 | 1.79E−05 | 1.225 | 2480 | 0.385 | 6.25 | 0.4 | 3 | 2.85 |
| 3 | f | 3.5 | 1.79E−05 | 1.225 | 2480 | 0.385 | 6.25 | 0.4 | 3 | 2.85 |
| 4 | u | 3.5 | 1.79E−05 | 1.225 | 2480 | 0.385 | 6.25 | 0.4 | 3 | 2.85 |
| 5 | u | 3.5 | 1.79E−05 | 1.225 | 2480 | 0.385 | 12.5 | 0.4 | 3 | 2.85 |
| 6 | u | 3.5 | 1.79E−05 | 1.225 | 2000 | 0.385 | 12.5 | 0.4 | 3 | 2.47 |
| 7 | u | 3.5 | 1.79E−05 | 1.5925 | 2480 | 0.385 | 12.5 | 0.4 | 3 | 2.61 |
| 8 | u | 3.5 | 1.79E−05 | 1.225 | 2480 | 0.385 | 12.5 | 1 | 7 | 2.85 |
| 9 | u | 3.25 | 1.79E−05 | 1.225 | 2480 | 0.385 | 6.25 | 0.4 | 3 | 2.85 |
| 10 | u | 3.75 | 1.79E−05 | 1.225 | 2480 | 0.44 | 6.25 | 0.4 | 3 | 3.25 |
| 11 | u | 2.75 | 4.45E−05 | 0.3105 | 2480 | 0.2555 | 12.5 | 0.4 | 3 | 1.53 |
| 12 | f | 3.75 | 1.79E−05 | 1.225 | 2480 | 0.44 | 12.5 | 0.4 | 3 | 3.25 |
| 13 | f | 2.75 | 1.79E−05 | 1.225 | 2480 | 0.2555 | 3.125 | 0.4 | 3 | 1.87 |
| 14 | f | 2.75 | 4.32E−05 | 0.324 | 2480 | 0.2555 | 3.125 | 0.4 | 3 | 1.56 |
| 15 | f | 2.75 | 1.79E−05 | 1.225 | 2480 | 0.2555 | 3.125 | 0.4 | 3 | 1.87 |
| 16 | u | 2.75 | 4.45E−05 | 0.3105 | 2480 | 0.2555 | 12.5 | 1 | 7 | 1.53 |
| 17 | u | 2.75 | 4.45E−05 | 0.3105 | 2480 | 0.2555 | 12.5 | 3 | 14 | 1.53 |
| 18 | u | 2.75 | 4.45E−05 | 0.3105 | 2480 | 0.2555 | 12.5 | 3 | 14 | 1.53 |
| 19 | u | 2 | 4.45E−05 | 0.3105 | 2480 | 0.2555 | 12.5 | 3 | 14 | 1.53 |
| 20 | u | 5 | 4.45E−05 | 0.3105 | 2480 | 0.2555 | 12.5 | 3 | 14 | 1.53 |
| 21 | u | 5 | 4.45E−05 | 0.3105 | 2480 | 0.44 | 12.5 | 3 | 14 | 3.37 |
| 22 | u | 5 | 4.45E−05 | 0.3105 | 2480 | 0.15 | 12.5 | 3 | 14 | 0.615 |
| 23 | u | 5 | 3.83E−05 | 0.3986 | 2480 | 0.2555 | 12.5 | 3 | 14 | 1.64 |
| 24 | u | 8 | 4.45E−05 | 0.3105 | 2480 | 0.2555 | 12.5 | 3 | 14 | 1.53 |
| 25 | u | 8 | 4.45E−05 | 0.3105 | 2480 | 0.2555 | 12.5 | 3 | 14 | 1.53 |
| 26 | u | 8 | 4.45E−05 | 0.3105 | 2480 | 0.2555 | 12.5 | 6 | 30 | 1.53 |
| 27 | o | 0.8 | 1.79E−05 | 1.225 | 2480 | 0.656 | 5 | 0.9 | 2 | 4.69 |
| 28 | u | 3.5 | 1.79E−05 | 1.225 | 2480 | 0.001 | 12.5 | 0.4 | 3 | 6.76 |
| 29 | u | 3.5 | 1.79E−05 | 0.8575 | 2480 | 0.385 | 12.5 | 0.4 | 3 | 3.22 |
| 30 | u | 3.5 | 2.79E−05 | 1.225 | 2480 | 0.385 | 12.5 | 0.4 | 3 | 2.45 |
| 31 | u | 3.5 | 7.90E−06 | 1.225 | 2480 | 0.385 | 12.5 | 0.4 | 3 | 3.61 |
| 32 | o | 0.8 | 4.45E−05 | 0.3105 | 2480 | 0.656 | 5 | 0.9 | 2 | 5.5 |
| 33 | o | 0.8 | 1.79E−05 | 0.3105 | 2480 | 0.656 | 5 | 0.9 | 2 | 7.67 |
| 34 | o | 0.8 | 4.45E−05 | 1.225 | 2480 | 0.656 | 5 | 0.9 | 2 | 3.59 |
| 35 | u | 1.5 | 1.79E−05 | 1.225 | 2480 | 0.385 | 12.5 | 0.4 | 3 | 2.85 |
| 36 | o | 0.8 | 1.79E−05 | 1.225 | 2480 | 0.656 | 5 | 0.9 | 2 | 4.69 |
| 37 | o | 2.2 | 1.79E−05 | 1.225 | 2480 | 0.2555 | 10 | 0.4 | 3 | 1.86 |
| 38 | o | 3.3 | 1.79E−05 | 1.225 | 2480 | 0.44 | 10 | 0.4 | 3 | 3.25 |
| 39 | o | 1.8 | 1.79E−05 | 1.225 | 1800 | 0.2555 | 10 | 0.4 | 3 | 1.49 |
| 40 | o | 2.75 | 1.79E−05 | 1.225 | 1800 | 0.44 | 10 | 0.4 | 3 | 2.63 |
| 41 | o | 0.7 | 4.45E−05 | 1.225 | 2480 | 0.44 | 10 | 0.4 | 3 | 2.35 |
| 42 | o | 1.4 | 4.45E−05 | 1.225 | 1800 | 0.2555 | 10 | 0.4 | 3 | 0.93 |
| 43 | o | 2.2 | 4.45E−05 | 1.225 | 1800 | 0.44 | 10 | 0.4 | 3 | 1.87 |
| 44 | o | 1.8 | 4.45E−05 | 1.225 | 2480 | 0.2555 | 10 | 0.4 | 3 | 1.2 |
| 45 | o | 0.5 | 1.79E−05 | 1.225 | 2480 | 0.2555 | 10 | 0.4 | 3 | 1.86 |
| 46 | o | 1 | 1.79E−05 | 1.225 | 2480 | 0.44 | 10 | 0.4 | 3 | 3.25 |
| 47 | o | 0.6 | 1.79E−05 | 1.225 | 1800 | 0.2555 | 10 | 0.4 | 3 | 1.49 |
| 48 | o | 1 | 1.79E−05 | 1.225 | 1800 | 0.44 | 10 | 0.4 | 3 | 2.63 |
| 49 | o | 0.8 | 4.45E−05 | 1.225 | 2480 | 0.44 | 10 | 0.4 | 3 | 2.35 |
| 50 | o | 0.3 | 4.45E−05 | 1.225 | 1800 | 0.2555 | 10 | 0.4 | 3 | 0.931 |
| 51 | o | 0.6 | 4.45E−05 | 1.225 | 1800 | 0.44 | 10 | 0.4 | 3 | 1.87 |
| 52 | o | 0.3 | 4.45E−05 | 1.225 | 2480 | 0.2555 | 10 | 0.4 | 3 | 1.2 |
| 53 | o | 0.44 | 1.79E−05 | 1.225 | 2480 | 0.2555 | 10 | 0.4 | 3 | 1.86 |
| 54 | o | 0.44 | 1.79E−05 | 1.225 | 2480 | 0.2555 | 10 | 0.4 | 3 | 1.86 |
| 55 | o | 0.66 | 1.79E−05 | 1.225 | 2480 | 0.44 | 10 | 0.4 | 3 | 3.25 |
| 56 | o | 0.4 | 1.79E−05 | 1.225 | 1800 | 0.2555 | 10 | 0.4 | 3 | 1.49 |
| 57 | o | 0.3 | 4.45E−05 | 0.3105 | 2480 | 0.15 | 10 | 0.4 | 3 | 0.615 |
| 58 | o | 0.3 | 4.45E−05 | 0.3105 | 2480 | 0.2555 | 10 | 0.4 | 3 | 1.53 |
| 59 | o | 0.5 | 4.45E−05 | 0.3105 | 2480 | 0.2555 | 10 | 0.4 | 3 | 1.53 |
| 60 | o | 0.7 | 4.45E−05 | 0.3105 | 2480 | 0.2555 | 10 | 0.4 | 3 | 1.53 |
| 61 | u | 0.7 | 4.45E−05 | 0.3105 | 2480 | 0.2555 | 10 | 0.4 | 3 | 1.53 |
| 62 | o | 1 | 4.45E−05 | 0.3105 | 2480 | 0.2555 | 10 | 0.4 | 3 | 1.53 |
| 63 | o | 1.3 | 4.45E−05 | 0.3105 | 2480 | 0.2555 | 10 | 0.4 | 3 | 1.53 |
| 64 | o | 1.6 | 4.45E−05 | 0.3105 | 2480 | 0.2555 | 10 | 0.4 | 3 | 1.53 |
| 65 | o | 2 | 4.45E−05 | 0.3105 | 2480 | 0.2555 | 10 | 0.4 | 3 | 1.53 |
| 66 | o | 1.6 | 4.45E−05 | 0.3105 | 2480 | 0.44 | 10 | 0.4 | 3 | 3.37 |
| 67 | o | 0.7 | 4.45E−05 | 0.3105 | 1800 | 0.2555 | 10 | 0.4 | 3 | 1.15 |
| 68 | o | 1 | 4.45E−05 | 1.225 | 2480 | 0.2555 | 10 | 0.4 | 3 | 1.2 |
| 69 | o | 1.6 | 1.79E−05 | 0.3105 | 2480 | 0.2555 | 10 | 0.4 | 3 | 2.7 |

Parameters: gas superficial velocity $U_0$, gas viscosity $\mu_g$, gas density $\rho_g$, solids density $\rho_s$, particle diameter $d_p$ (monodisperse), mesh spacing $\Delta x_{mesh}$, riser width $w$, riser height $h$, and the terminal velocity of a particle $v_t$. In the table, 'u' denotes uniform gas inlet velocity, 'o' a distributor with separate nozzles, and 'f' a distributor where the effect of nozzles on the gas velocity profile is given by a function.

**Table 2**
The models and parameters used in the simulations.

Gas phase (continuity and momentum equations)

$$\frac{\partial}{\partial t}\left(\alpha_g\rho_g\right)+\nabla\cdot\left(\alpha_g\rho_g\boldsymbol{u}_g\right)=0$$

$$\frac{\partial}{\partial t}\left(\alpha_g\rho_g\boldsymbol{u}_g\right)+\nabla\cdot\left(\alpha_g\rho_g\boldsymbol{u}_g\boldsymbol{u}_g\right)=-\alpha_g\nabla p+\nabla\cdot\boldsymbol{\tau}_g+\alpha_g\rho_g\boldsymbol{g}+K_{gs}(\boldsymbol{u}_s-\boldsymbol{u}_g)$$

Solid phase (continuity and momentum equations)

$$\frac{\partial}{\partial t}(\alpha_s\rho_s)+\nabla\cdot(\alpha_s\rho_s\boldsymbol{u}_s)=0$$

$$\frac{\partial}{\partial t}(\alpha_s\rho_s\boldsymbol{u}_s)+\nabla\cdot(\alpha_s\rho_s\boldsymbol{u}_s\boldsymbol{u}_s)=-\alpha_s\nabla p-\nabla p_s+\nabla\cdot\boldsymbol{\tau}_s+\alpha_s\rho_s\boldsymbol{g}+K_{gs}(\boldsymbol{u}_g-\boldsymbol{u}_s)$$

Granular energy equation

$$\frac{3}{2}\left[\frac{\partial}{\partial t}(\alpha_s\rho_s\Theta_s)+\nabla\cdot(\alpha_s\rho_s\boldsymbol{u}_s\Theta_s)\right]=(-p_s\mathbf{I}+\boldsymbol{\tau}_s):\nabla\boldsymbol{u}_s+\nabla\cdot\left(k_{\Theta_s}\nabla\Theta_s\right)-\gamma_{\Theta_s}+\phi_{gs}$$

Diffusion coefficient for granular energy (Syamlal et al. [14])

$$k_{\Theta_s}=\frac{15d_s\rho_s\alpha_s\sqrt{\Theta_s\pi}}{4(41-33\eta)}\left[1+\frac{12}{5}\eta^2(4\eta-3)\alpha_s g_{0,ss}+\frac{16}{15\pi}(41-33\eta)\eta\alpha_s g_{0,ss}\right],\ \text{where}\ \eta=\frac{1}{2}(1+e_{ss})$$

Collisional dissipation of energy [15]

$$\gamma_{\Theta_s}=\frac{12(1+e_{ss}^2)g_{0,ss}}{d_s\sqrt{\pi}}\alpha_s^2\rho_s\Theta_s^{3/2}$$

Energy exchange between the gas and solid phase [15]

$$\phi_{gs}=-3K_{gs}\Theta_s$$

Phase stress–strain tensors

$$\tau_g=\alpha_g\mu_g\left(\nabla\boldsymbol{u}_g+\nabla\boldsymbol{u}_g^T\right)-\frac{2}{3}\alpha_g\mu_g\left(\nabla\cdot\boldsymbol{u}_g\right)\mathbf{I}$$

$$\tau_s=\alpha_s\mu_s\left(\nabla\boldsymbol{u}_s+\nabla\boldsymbol{u}_s^T\right)+\alpha_q\left(\lambda_s-\frac{2}{3}\mu_s\right)(\nabla\cdot\boldsymbol{u}_s)\mathbf{I}$$

Solid shear viscosity $\mu_s=\mu_{s,col}+\mu_{s_{kin}}+\mu_{s,fr}$ [14,16]

$$\mu_s=\frac{4}{5}\alpha_s\rho_s d_s g_{0,ss}(1+e_{ss})\left(\frac{\Theta_s}{\pi}\right)^{\frac{1}{2}}+\frac{\alpha_s\rho_s d_s\sqrt{\Theta_s\pi}}{6(3-e_{ss})}\left[1+\frac{2}{5}(1+e_{ss})(3-e_{ss}-1)\alpha_s g_{0,ss}\right]+\frac{p_s\sin\phi}{2\sqrt{I_{2D}}}$$

Granular bulk viscosity [15]

$$\lambda_S=\frac{4}{3}\alpha_S\rho_S d_s g_{0,ss}(1+e_{ss})\left(\frac{\Theta_s}{\pi}\right)^{1/2}$$

Solids pressure [15]

$$p_s=\alpha_s\rho_s\Theta_s+2\rho_s(1+e_{ss})\alpha_s^2 g_{0,ss}\Theta_s$$

Radial distribution function [17]

$$g_{0,ss}=\left[1-\left(\frac{\alpha_s}{\alpha_{s,\max}}\right)^{\frac{1}{3}}\right]^{-1}$$

Drag model [9], based on Ergun [18] and Wen and Yu [8])

When $\alpha_g > 0.8$:

$$K_{gs}=\frac{3}{4}C_d\frac{\alpha_g\alpha_s\rho_g|\boldsymbol{u}_g-\boldsymbol{u}_s|}{d_s}a_g^{-2.65}$$

$$C_d=\begin{cases}\frac{24}{Re}[1+0.15(\mathrm{Re})^{0.687}, Re<1000\\ 0.44, Re\geq 1000\end{cases}$$

$$Re=\frac{\alpha_g\rho_g|\boldsymbol{u}_g-\boldsymbol{u}_s|d_s}{\mu_g}$$

When $\alpha_g \leq 0.8$:

$$K_{gs}=150\frac{\alpha_s(1-\alpha_g)\mu_g}{\alpha_g d_s^2}+1.75\frac{\rho_g\alpha_s|\boldsymbol{u}_g-\boldsymbol{u}_s|}{d_s}$$

used and for the volume fraction equation the convection scheme was QUICK. For the pressure–velocity coupling the phase coupled SIMPLE was used. The time step in the first order implicit time-stepping procedure was 0.001 s for the 10 mm and coarser meshes and 0.0005 s for the 6.25 mm and finer meshes. Comparisons [19] with measurements of solids volume fraction profiles, determined from the local gray scale values in video images, have been previously carried out for some of the simulations of a 0.4-m-wide pseudo-2D CFB. The measurement and simulation results were in good qualitative agreement and even quantitatively the results were reasonably good considering that the simulations were carried out in 2D. Thus the chosen transient simulation approach can be considered sufficiently accurate to produce qualitatively representative data for evaluation of the new modeling strategy for filtered gas–solid drag force.

For each case, approximately 5 s was simulated before initialization of the time averaging and at least a further 120 s of flow time was simulated to compute the averages, which is sufficient to guarantee a satisfactory convergence of the time-averaged properties in most of the flow regions. Typical bubbling frequencies in BFBs are of the order of 1–10 Hz [20] and similar fluctuation frequencies are also common in CFBs. Also on this basis the 120-s averaging time can be considered adequate. However, for the very dilute parts of the BFB freeboard region, where bursts of particles only occasionally occur, the averaging period is not sufficient, a limitation that has to be taken into account in the analysis of the simulation results.

## 3. Analysis and pre-processing of the transient simulation results

### 3.1. Time averaging

Results from each transient simulation were time-averaged to determine the average flow properties and the average drag force in each computational cell. As in the previous study [10], the analysis was carried out for the dominating, vertical component of the drag force. A closure for the time-averaged drag force can be written in the form

$$\overline{K_{gs}\left(u_{g,y}-u_{s,y}\right)}=C_{\mathrm{drag}}K_{gs}^{*}\left(U_{g,y}-U_{s,y}\right) \tag{1}$$

where $u_{g,y}$ and $u_{s,y}$ are the instantaneous gas and solid phase vertical velocity components and $U_{g,y}$ and $U_{s,y}$ the corresponding mass-weighted time-averaged (Favre averaged) velocity components. The coefficient $C_{\mathrm{drag}}$ in Eq. (1) is a drag correction coefficient, for which a correlation is to be developed. $K_{gs}^{*}$ is the inter-phase momentum transfer coefficient calculated on the basis of the time-averaged velocities and volume fractions using a combination of Wen and Yu [8] and Ergun [18] drag laws. However, instead of using the combination approach of Gidaspow's [9] drag law a smoother transition between the drag laws, suggested by Niemi et al. [21], was used to calculate $K_{gs}^{*}$. In this model a linear transformation between the Ergun and Wen–Yu models occurs in a solid volume fraction range of 0.4–0.5, which is within the region recommended by Leboreiro et al. [22].

The value of $C_{\mathrm{drag}}$ in each point in the flow field can be calculated from Eq. (1) by time averaging the drag force, the solid volume fraction and the gas and solid velocities over the simulation time of a transient simulation. This kind of data was collected for each of the simulations. A filtering process was carried out on the data collection stage. For very low values of the slip velocity, the computed $C_{\mathrm{drag}}$ can become unreasonably large due to the stochastic nature of the data and the finite averaging periods. A maximum limit for $C_{\mathrm{drag}}$ was set to 5. Above this level the data were chaotic and the number of observations was small. All negative values were rejected for the same reasons. The data of the solid return channel were also omitted from the analysis since the flow structure in this region significantly deviates from the typical conditions of interest.

### 3.2. Effects of the fluidization velocity

In the previous study by Kallio et al. [10], only results from CFB simulations were analyzed and it was concluded that fluidization velocity has only a minor effect on $C_{\mathrm{drag}}$. However, when the fluidization velocity significantly reduces from the typical CFB values, the flow pattern drastically changes and instead of being characterized by clusters and strands surrounded by dilute suspension, the flow shows voids and bubbles inside a dense suspension. This change in flow conditions is illustrated in Figs. 2 and 3 for simulations with superficial gas velocity ranging from 0.3 to 2 m/s. The change in flow pattern is expected to have a large effect on the average drag force and on $C_{\mathrm{drag}}$.

The $C_{\mathrm{drag}}$ values calculated in all the mesh points (excluding the return channel) are displayed as a function of the local average solid volume fraction in Fig. 4. A gradual change in the pattern can be observed when the fluidization state gradually changes from BFB conditions (cases with $U_0 \leq 0.5$ m/s) to typical CFB riser flow (cases with $U_0 \geq 1.6$ m/s). At high solid concentrations in bubbling bed conditions $C_{\mathrm{drag}}$ appears to be independent of the average solid volume fraction $\alpha_s$. Since the highest $\alpha_s$ values typically occur close to walls and in corners, this behavior can be attributed to wall effects. At approximately $\alpha_s = 0.2 - 0.3$, i.e. typical values inside a bubbling bed, a similar poor coupling between $C_{\mathrm{drag}}$ and $\alpha_s$ can be observed. Starting from $\alpha_s = 0.05$, a value corresponding to the zone near bed surface (Fig. 3), $C_{\mathrm{drag}}$ first exceeds one and, as $\alpha_s$ decreases, $C_{\mathrm{drag}}$ decreases to very low values as $\alpha_s$ approaches $10^{-5}$. As $\alpha_s$ is further reduced in the freeboard to

values close to 0 $C_{drag}$ again increases. A large scatter in $C_{drag}$ is visible in the freeboard region at the dilute end of the scale. These very low $\alpha_s$ values represent regions into which only a very limited number of bursts of particles have risen during the 120-s averaging period and consequently the averages are not representative. At high fluidization velocities in CFB conditions $C_{drag}$ shows a clear dependency on $\alpha_s$, except in the dense end of the scale, which corresponds to the acceleration zone in the bottom bed [10]. At higher superficial velocities, the $\alpha_s$ range in which $C_{drag}$ is almost constant is wider.

Fig. 5 analyses the data from the simulation 65 with the aim to identify the regions from which the different $C_{drag}$ patterns in CFB conditions originate. First, the bottom region up to a height of 0.1 m is removed from the depicted data points. This elimination of data reduces the scattering of $C_{drag}$ at higher $\alpha_s$ values. Next, the regions with a wall distance below selected thresholds (0.01, 0.02 and 0.05 m, respectively) are removed. From the results it can be concluded that the major part of the scattering in the data originates from the wall layer. In particular the values in the grid cells adjacent to the walls show a distinct pattern that completely deviates from the rest of the data.

A similar analysis was carried out in BFB conditions for the simulation 59 whose results are shown in Fig. 6. Removal of the data from the lowermost part below a height of 0.1 m reduces the scatter in the dense end of $\alpha_s$ scale. The large scatter in the dilute end vanishes when data above 0.9 m, corresponding to the freeboard region, is removed. The analysis shown in Fig. 6 demonstrates that low $C_{drag}$ values are found in the regions adjacent to the wall, which are intimately different from the rest of the flow domain.

### 3.3. Pre-processing of the data

The complexity of the behavior of $C_{drag}$ as a function of solid volume fraction is evident in Fig. 4. In particular, the pattern in the region adjacent to the wall is completely different from that of the rest of the flow domain. Thus a need for a separate correlation for the wall region was indicated. To simplify the modeling task the region up to 2–5 cm from the wall (depending on the case) was omitted from further analysis. Similarly, in the bottom region, scatter in the data increases as we move toward the air distributor and thus the region from the bottom up to 0.1 m was excluded. In BFB simulations, the scatter in the data in dilute conditions is a result of the inadequate averaging period in the freeboard region. Thus freeboard data were also omitted. Since the location of the bed surface varies from case to case, this removal threshold was separately set for each case. As an example, Fig. 7 shows the cleaned data used for modeling in Cases 59, corresponding to typical BFB conditions, and 65, corresponding to typical CFB conditions. Compared to the original data shown in Fig. 6, the scatter in the data has significantly reduced.

### 3.4. Effect of the air distributor

In some of the simulations, the gas flow entered uniformly through the bottom edge of the computational domain while in others, especially at lower gas velocities, gas was introduced through discrete nozzles separated by 0.05-m space intervals. In CFB conditions, our previous experiences have shown that the type of the gas-flow inlet boundary condition at the bottom plays only a very limited local role. This was also confirmed in the present study by comparing results from Cases 2 and 3 of Table 1 which differ only in the way air enters the bed at riser bottom. In bubbling beds, average bubble size as a function of height is commonly expressed in terms of the initial bubble size, which in turn depends on the nozzle diameter [20]. Thus in BFB conditions, the air distributor design can have a major effect on suspension behavior and hence also on $C_{drag}$. Fig. 8 illustrates this effect by comparing the $C_{drag}$ values determined from simulations 60 (with orifices) and 61 (uniform gas velocity). Uniform air velocity at the bottom leads to $C_{drag}$ values closer to unity in the solid concentration range corresponding to the center of the bed, which suggests more uniform flow conditions when no orifices are used. The effect of the air distributor design is thus clear, implying that in the bubbling bed region the drag correction function should take into account the effect of the air distributor design. In the present study, most of the BFB data have been obtained with the aforementioned air distributor. In industrial BFBs and CFBs air distributor designs differ from the present simple one. This represents a possible source of inaccuracy, if a drag law based on the results of the present work would be applied in such industrial applications.

### 3.5. Parametric effects

In Kallio et al. [10] effects of material properties on $C_{drag}$ in CFB conditions were analyzed. Particle size was found to have an increasing effect on $C_{drag}$ while gas viscosity had a reducing effect. The effect of solid density was clear but less straightforward. In BFB conditions, a change in

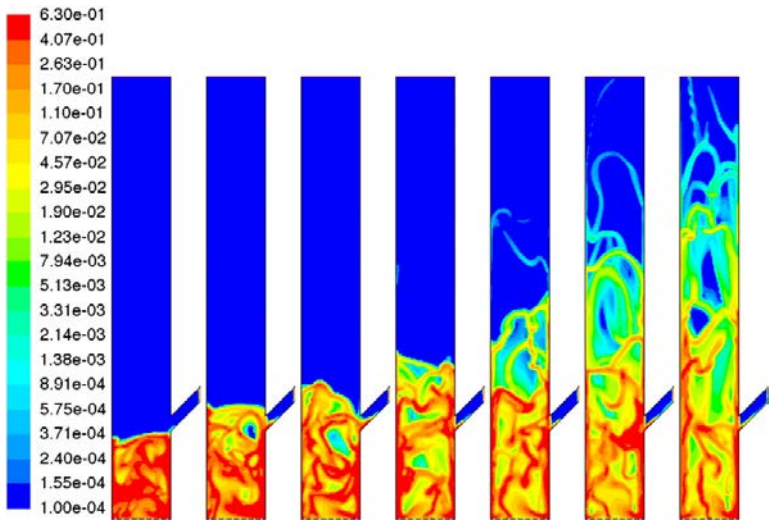


**Fig. 2.** Instantaneous solid volume fraction fields in simulations (from the left) 58, 59, 60, 62, 63, 64 and 65 at fluidization velocities 0.3, 0.5, 0.7, 1, 1.3, 1.6 and 2 m/s, respectively.

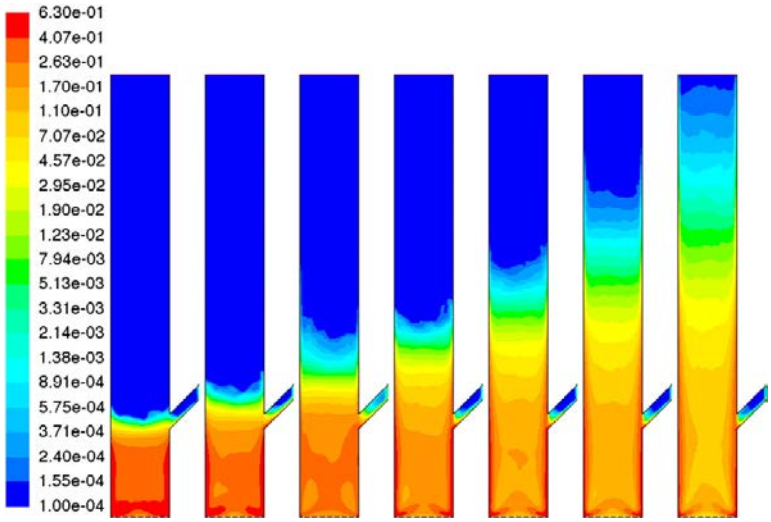


**Fig. 3.** Time-averaged solid volume fraction fields in simulations (from the left) 58, 59, 60, 62, 63, 64 and 65 at fluidization velocities 0.3, 0.5, 0.7, 1, 1.3, 1.6 and 2 m/s, respectively.

material properties leads to a change in bubble size and gas and solid velocities. Even in CFB conditions material properties affect the flow pattern, e.g. cluster properties, but not to the same extent as in a BFB. The low gas velocity in BFB and TFB conditions makes the processes more sensitive to the changes in material properties, since a change in the fluidization mode between BFB and TFB conditions can take place. Thus it is not equally easy to evaluate the effects of material properties at low gas velocities. Fig. 9a illustrates the effect of gas viscosity (Cases 34 and 36 in Table 1). The observed effect is negative, i.e. an increase in the viscosity leads to a lower $C_{drag}$. In Fig. 9b (Cases 52 and 58) the effect of gas density is shown to be small. A similar result was obtained in CFB conditions [10] and it was concluded that gas density can be omitted from the set of input parameters of a drag correction function. Fig. 10a (Cases 46 and 48) shows a positive effect of solids density while the opposite trend is observed in Fig. 10b (Cases 60 and 67). Thus solid density does not seem to have a simple independent effect on the results. Fig. 10c shows a positive effect of the particle size. The effects of the particle size and gas viscosity were evaluated only in a one case, i.e. with a single set of other operational conditions. A larger number of comparisons should be carried out to confirm whether the effects of particle size and gas viscosity are independent or affected by other flow parameters.

## 4. Empirical modeling

### 4.1. Data sampling

Since each computational cell produces one observation in the data set, the amount of data collected from each of the simulations is unnecessarily large for model development. Even after clean-up of the data and

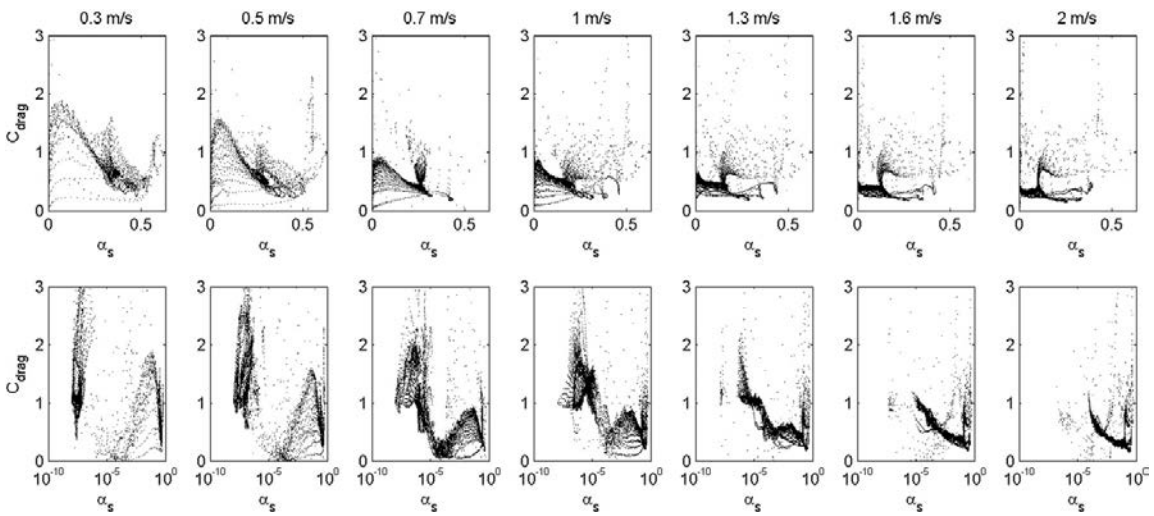


**Fig. 4.** Drag correction coefficient $C_{drag}$ as a function of the solid volume fraction $\alpha_s$ in linear (top) and logarithmic (bottom) scales in simulations (from the left) 58, 59, 60, 62, 63, 64 and 65 at fluidization velocities 0.3, 0.5, 0.7, 1, 1.3, 1.6 and 2 m/s, respectively.

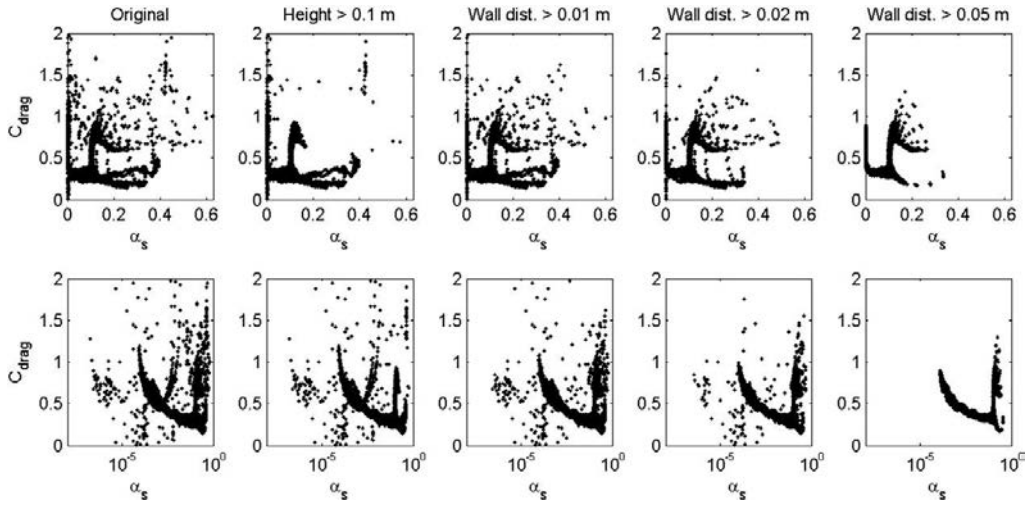


**Fig. 5.** Analysis of regional effects on $C_{drag}$ in CFB conditions in Case 65 in linear (top) and logarithmic (bottom) scales. The leftmost image shows the original data and in the other images, different regions are removed from the plots. From left to right, the removed regions are: the bottom section up to 0.1 m, the wall region up to 1 cm from the wall, the wall region up to 2 cm from the wall, and the wall region up to 5 cm from the wall.

removal of data from entrance, exit and wall regions (see Section 3.2), thousands to tens of thousands of data points were collected from each of the 69 simulations. In order to reduce the amount of data to a more manageable quantity without losing relevant information, data used for modeling were randomly picked from each of the simulations. Since most of the points come from the central region of the riser, randomly picking from the entire region would mainly collect data from the central regions. In order to avoid such pre-conditioning, the simulation domain was divided into bottom, side and central regions, from which data were successively picked. A relatively larger amount of data was sampled from the dense regions at bed bottom and closer to walls, since in those zones the behavior of $C_{drag}$ is more complex. Fig. 11 shows the picked points for Cases 59 and 65. Finally about 5000 points were included in the data set used for the empirical modeling. The full data set was used only for testing the derived correlations.

### 4.2. Model structure and the parameter estimation procedure

To allow the developed correlation to freely adjust to the input data, a model structure based on a combination of a number of logistic sigmoid functions was used in this work for nonlinear regression. This model structure is commonly used in neural network modeling [23]. The model can be written as

$$C_{\mathrm{drag,pred.}} = b_0 + \sum_{i=1}^{N_\sigma} b_i\, \sigma(z_i) \tag{2}$$

$$z_i = a_0 + \sum_{i=1}^{N_{in}} a_i\, x_i \tag{3}$$

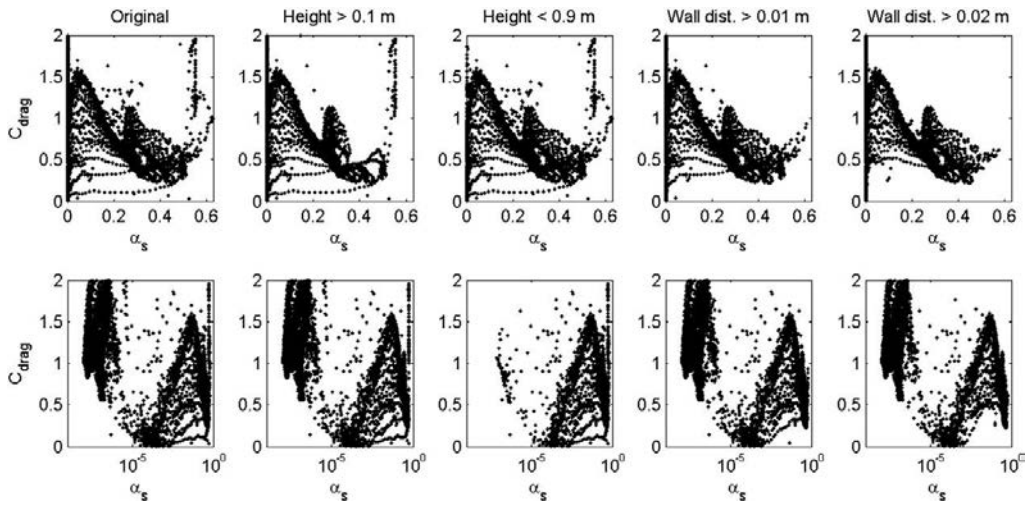


**Fig. 6.** Analysis of regional effects in BFB conditions in Case 59 in linear (top) and logarithmic (bottom) scales. The leftmost images show the original data and in the rest, different regions are removed from the data set. From left to right, the removed regions are: the bottom section up to 0.1 m, the freeboard region above 0.9 m, the wall region up to 1 cm from the wall, and the wall region up to 2 cm from the wall.

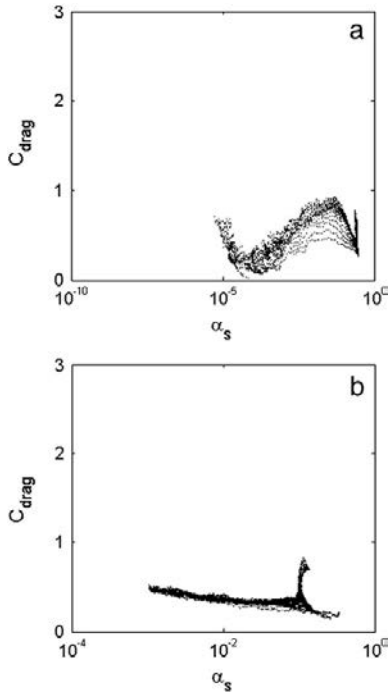


**Fig. 7.** Cleaned data (a) in Case 59 (BFB conditions) and (b) in Case 65 (CFB conditions).

where $a_i$ and $b_i$ denote model parameters and $x_i$ the $N_{in}$ input variables. The logistic sigmoid function that produces values between 0 and 1 is given by

$$\sigma(z_i) = \frac{1}{1+e^{-z_i}} \tag{4}$$

The input variables considered in this work were the material properties, the solid volume fraction, gas and solid velocities, the slip velocity, the distance from the wall and the elevation, which are readily available in a simulation. Instead of solid volume fraction, the logarithm

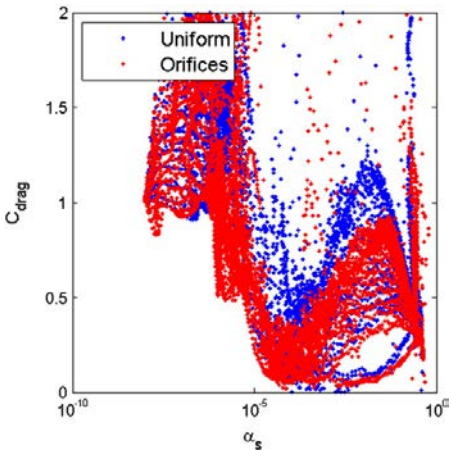


**Fig. 8.** Comparison of drag correction coefficient values in BFB conditions in Cases 60 (air enters through separate orifices) and 61 (a uniform gas inflow velocity at the bottom).

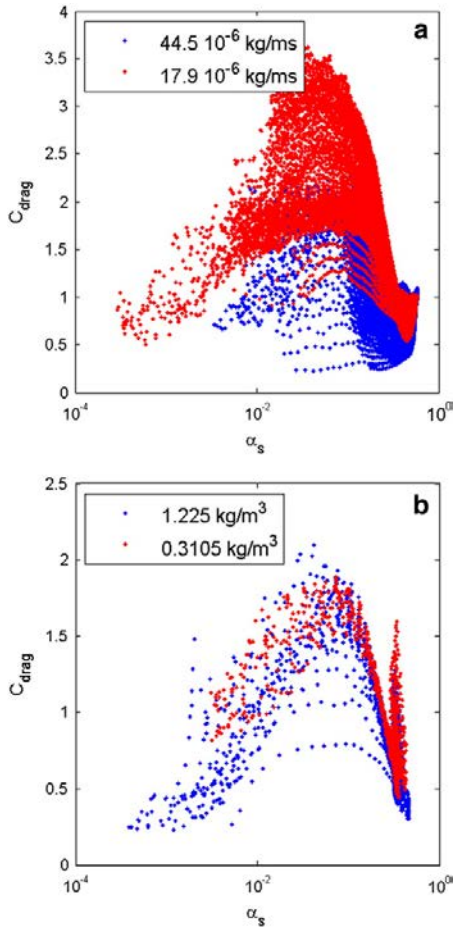


**Fig. 9.** Effects of (a) changed viscosity (Cases 34 and 36), and (b) changed gas density (Cases 52 and 58) in BFB conditions. From the original data set exit, entrance and wall region data have been excluded.

of solid volume fraction was used as an input parameter which makes it easier to express the steep gradients at low solid concentrations, shown in Fig. 10, with sigmoid functions.

The model parameters $(a_i, b_i)$ were determined by minimizing the prediction error $E$

$$E = \sum_{k}^{N_{obs}} \left( C_{drag,obs} - C_{drag,pred} \right)^2 \tag{5}$$

Parameter search was done with the Levenberg–Marquardt [24] method. The data used as the basis for modeling were quite limited and not of optimal quality, since only very few combinations of material properties were included. Thus special attention was paid to the robustness of the correlation. The correlation should not produce excessively large or small values in the points that were excluded from the data set used for parameter estimation. Thus some interpolation capabilities were desired. Some of the parameters $(a_i, b_i)$ were fixed to zero to reduce the complexity of the correlation and to improve its robustness. With a larger number of sigmoids and model parameters, prediction accuracy could improve for the actual data set but the correlation's ability to produce reasonable values would deteriorate in conditions that were

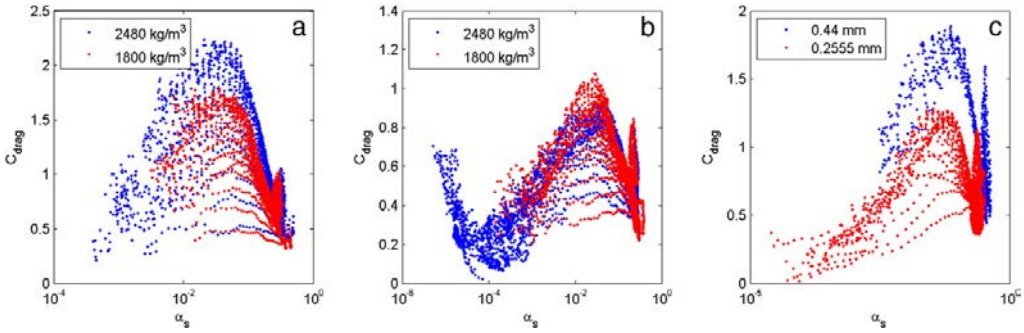


**Fig. 10.** Effects of changed solid density (a) in Cases 46 and 48 and (b) in Cases 60 and 67). (c) Effects of a changed particle size (Cases 57 and 58) in BFB conditions. From the original data set exit, entrance and wall region data have been excluded.

not included in the simulations carried out so far. Thus demands for robustness and accuracy need to be weighed against each other during the modeling process.

### 4.3. Modeling of the change from CFB to BFB conditions

As an initial test, data from 18 simulation cases with the same material properties (air at 850 ºC, solid density 2480 kg/m$^3$ particle size 0.255 mm) were chosen for modeling. The purpose of the test was to find the necessary parameters for describing the effect of the fluidization state. According to the initial parameter list of Kallio et al. [10], solid volume fraction, wall distance and slip velocity should suffice for the task when material properties are constant. However, a first trial made with these three input parameters did not produce a satisfactory correlation. We then introduced the height above the air distributor as the fourth variable, as the bubble size and velocity for bubbling beds are commonly expressed as a function of the height (e.g. Kunii and Levenspiel [20]). Fig. 12 shows the predicted and observed behavior in Cases 11, 16, 19, 59, 61, and 63 with the best correlation that was found based on the four input parameters. The number of parameters in the correlation was 25 and about 700 observations in the data set were picked from the 18 simulations used as the basis for modeling. The correlation was developed based on the cleaned data set (with no wall, bottom and freeboard data) but the comparisons between the observed and predicted $C_{drag}$ values in Fig. 12 are shown for the complete data sets to evaluate the correlation's robustness and ability to extrapolate. One measure of the goodness of the fit between observed and predicted values is the correlation coefficient $R$ (defined as the covariance of the two variables divided by the product of their standard deviations). The correlation coefficients for these cases are 0.74, 0.92, 0.94, 0.57, 0.82, and 0.69, respectively, calculated on the basis of the original data set covering the entire riser region. In BFB (Cases 59 and 61 in Fig. 12) and CFB (Cases 11, 16, and 19 in Fig. 12) conditions the fit is generally satisfactory but near the BFB surface and freeboard as well as in turbulent bed conditions a larger error is seen. The correlation has difficulties to describe the low values of $C_{drag}$ on the surface of a bubbling bed. At similar low volume fractions in CFB conditions $C_{drag}$ is close to unity while on the BFB surface $C_{drag}$ approaches zero. None of the input variables seems to be able to describe the difference in the flow behavior. Despite of this setback the modeling approach can be considered successful as it produces good results in a wide range of fluidized bed conditions.

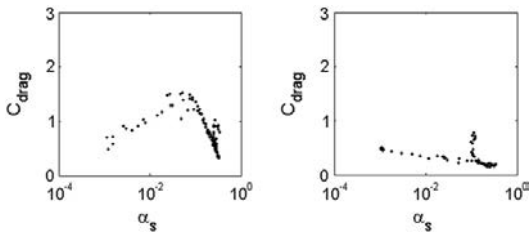


**Fig. 11.** Data points sampled from Cases 59 (BFB, left) and 65 (CFB, right).

Other correlations with alternative sets of input variables and a larger number of model parameters were tried but the results were not as good. Addition of complexity to the correlation showed slight improvement in the agreement between predicted and observed values but not enough to justify the increased number of model parameters, which in turn could result in a reduced robustness of the correlation.

### 4.4. Modeling with material properties as additional input variables

To account for changes in material properties, the data from all the 69 simulation were included for the development of the correlation. As a first tentative step, seven input variables were used, i.e. solid volume fraction, wall distance, elevation, slip velocity, gas viscosity, solids material density and particle size. All the correlations developed with these inputs encountered difficulties in reproducing $C_{drag}$ in BFB conditions and often produced clearly false maximum $C_{drag}$ in the bed region. The correlation between observed and predicted $C_{drag}$ was poor ($R < 0.7$). No results obtained with this set of input parameters are shown in the present paper. We then added an eighth input variable, the local gas velocity, and the correlation improved significantly. Several different configurations of the model structure given by Eqs. (2)–(4) were tried with different numbers of sigmoids and parameters. The best developed correlation that was reasonably accurate and at the same time sufficiently robust had 71 parameters. Fig. 13 shows the observed versus predicted $C_{drag}$ for all the points in the data set used for model development (the correlation coefficient between observed and predicted values was 0.96). The number of parameters in the model is large but not unreasonable considering that the correlation attempts to describe the effects of eight input variables, including their combined contributions. The number of observations (5000) in the data set used in the parameter estimation process is two orders of magnitude larger than the number of parameters. Thus the amount of data can be considered sufficient. However, the robustness of the correlation should still be checked by testing its behavior in conditions that were not included in those 5000 observations.

Fig. 14 compares the observed and predicted values in six different simulation cases. For qualitative assessment of the robustness of the correlation, the observations and predictions are shown for the full original data set (however, without data for the solids return duct). Fig. 14a, b, and c are for the same simulation cases (Cases 19, 59 and 63 in Table 1) as shown in Fig. 12. The predictions have deteriorated from what was obtained in Fig. 12 since the new parameters are no more optimized for the specific material property values. Correlation coefficients

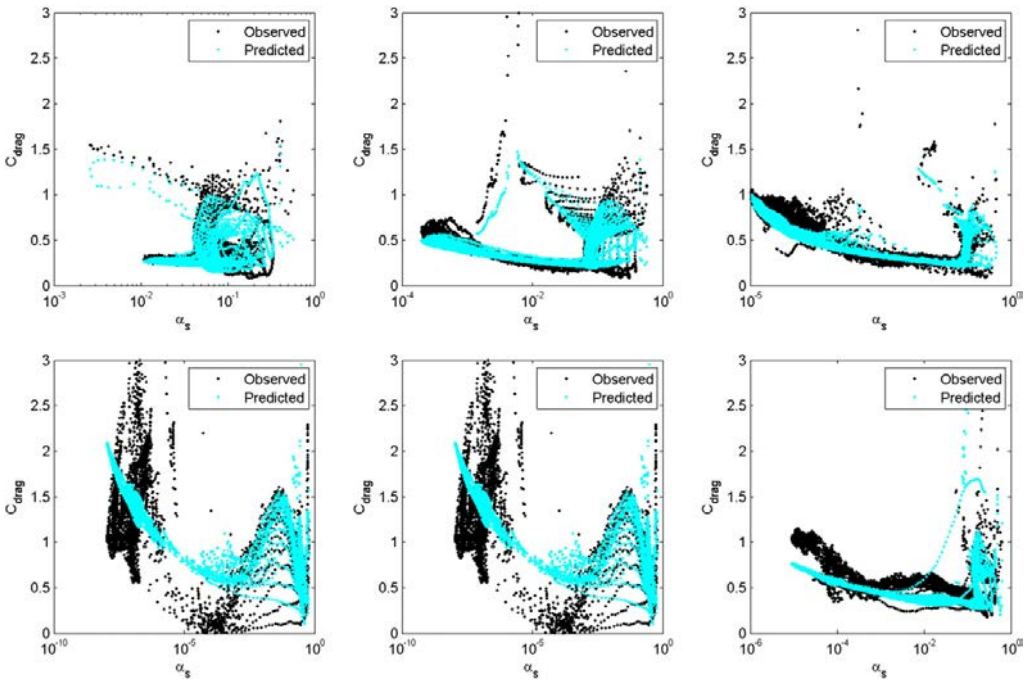


**Fig. 12.** The predicted and observed behavior in Cases 11 (top, left), 16, 19, 59 (bottom, left), 61, and 63 with the best found correlation based on four input parameters, i.e. the solid volume fraction, the slip velocity, the wall distance and the elevation.

calculated on the basis of the full original data sets were 0.81, 0.10, and 0.60, respectively, which all are lower than the corresponding values 0.94, 0.57, 0.69 obtained with the correlation developed in Section 4.3. Fig. 14d, e and f (Cases 6, 29 and 53 in Table 1) is for other material property values and shows a similar fit to the observed data with correlation coefficients 0.82, 0.76, and 0.02, respectively. For the BFB Cases 59 and 53, the correlation coefficients calculated on the basis of the full original data sets are very low. If the large amount of data from the dilute freeboard region ($\alpha_s < 10^{-5}$) is omitted, the correlation coefficients become 0.6728 (Case 59) and 0.87 (Case 53).

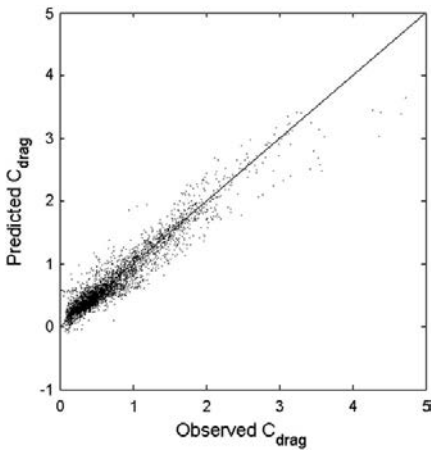


**Fig. 13.** The observed versus predicted $C_{drag}$ for all the instances in the data set used for model development.

### 4.5. Separate correlation for the dilute CFB conditions

The correlation developed on the basis of the full range of data, discussed in the previous section, proved to be far from an optimal fit at low solids concentrations. This is probably due to the difficulties related to trying to model both BFB and CFB conditions with the same correlation. In a simulation of a CFB, dilute suspension conditions prevail in the major part of the flow domain. Thus a big error in the drag force at low values of $\alpha_s$ can lead to serious errors in the predicted solids velocities and concentrations in a major part of the riser. To remedy this problem, a separate correlation was developed on the basis of data collected from CFB riser simulations in regions above 1.5-m height. The set of input variables could in this case be simplified by omitting gas velocity and the elevation. Thus the correlation for the limited dilute region is based on material properties (gas viscosity, solids density, particle size), solids volume fraction, slip velocity and wall distance. Again a number of correlation structures were tried and finally a correlation with acceptable accuracy and robustness was selected. The final correlation has only 14 parameters.

Fig. 15 shows the observed versus the predicted $C_{drag}$ for all the instances in the data set used for development of the correlation (the correlation coefficient between observed and predicted values is 0.96). As expected the predictions have significantly improved in the dilute range from what was obtained in Fig. 14, since no compromise was necessary between dilute conditions in a CFB and in the freeboard region of a BFB. In Fig. 14, this compromise led to systematically too low $C_{drag}$ values in the dilute regions of a CFB while no such systematic error can be seen in Fig. 15. As it is, the correlation is not generally usable since it behaves poorly in dense conditions unless it is combined with a correlation that works better in the dense bottom region. Fig. 16 shows results obtained with a correlation that, by means of linear and bilinear blending functions, combines the new correlation for dilute conditions in the upper parts of a CFB with the previous correlation of

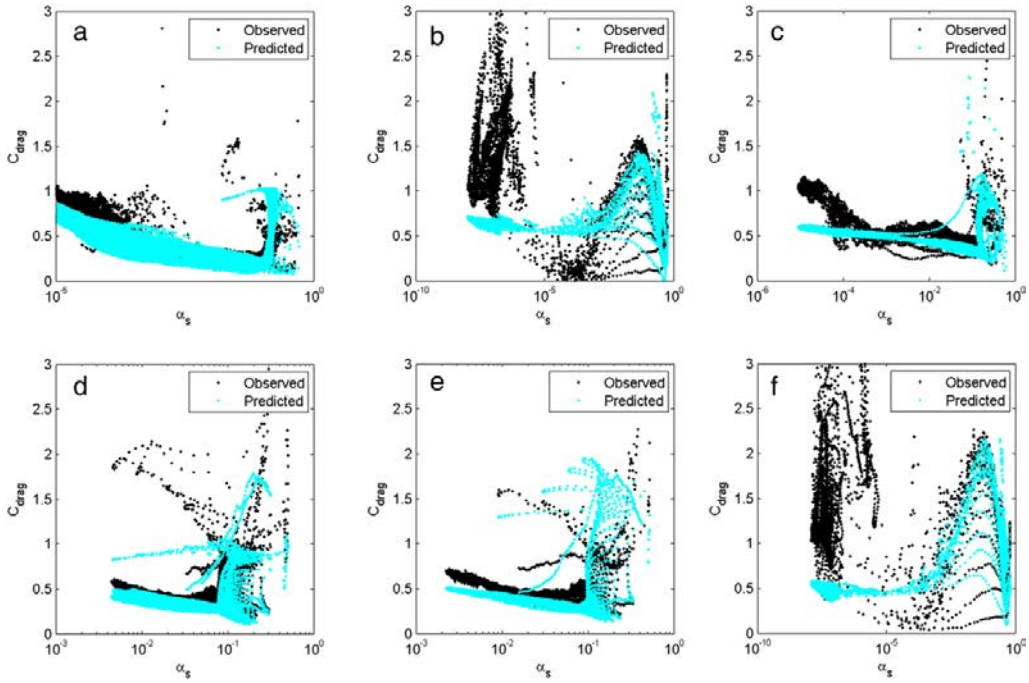


**Fig. 14.** The predicted and observed behavior in Cases 19 (a), 59 (b), 63 (c), 6 (d), 29 (e) and 53 (f) with the best found correlation based on eight input variables (the solid volume fraction, the slip velocity, the gas velocity, the solid density, the gas viscosity, the particle size, the elevation and the distance from the wall).

Section 4.4, which now is used only for the bottom bed and dense conditions. The two parameters that govern the switch from one correlation to the other and determine the value of the blending functions are the solid volume fraction and elevation. The blending functions are shown in Table 3.

The results shown in Fig. 16 for Cases 19, 59, 63, 6, 29 and 53 (same as in Fig. 14) are in general qualitatively correct. The correlation coefficients calculated on the basis of the full original data sets are 0.94, 0.37 (0.67 for data in the range $\alpha_s > 10^{-5}$), 0.83, 0.81, 0.77, and 0.09 (0.87 for $\alpha_s > 10^{-5}$), respectively, showing clear improvement compared to the results in Section 4.4. The values at the surface of a BFB (Fig. 16b and f) are still poorly predicted and in the dense end of the scale, large discrepancies between observed and predicted values occur in CFB conditions (Fig. 16a, d and e). However, the less well-reproduced values occur in the regions that were excluded from the data set used as basis for modeling. Thus deviations from observed values were expected. Since no order-of-magnitude errors occur in these regions, the correlation appears to be reasonably robust.

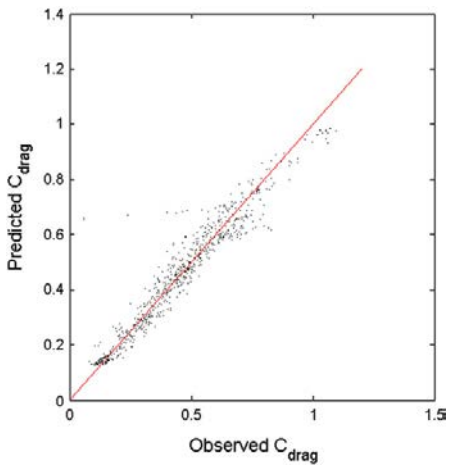


**Fig. 15.** Predicted versus observed $C_{drag}$ for all the instances in the data set for dilute CFB conditions used for model development.

To illustrate the correlation's sensitivity to the changes in material properties, the observed and predicted $C_{drag}$ values are depicted in Fig. 17 for two BFB cases with different particle sizes and in Fig. 18 for two CFB cases with different solid densities. The trends of the parametric effects are predicted correctly in Figs. 17 and 18.

### 4.6. Testing of the correlation

Although special attention was paid to the robustness of the derived correlations, it is useful also to compare the predicted results with observations in conditions that were not included in the data set used for derivation of the parameters. One additional case was simulated in CFB and one in BFB conditions in the 0.4 m wide geometry of Fig. 1 to test the performance of the correlation presented in Section 4.5. In both cases the material properties were as follows: particle size 0.3 mm, solids material density 2200 kg/m$^3$, gas density 1 kg/m$^3$, and solids viscosity $2.2 \cdot 10^{-5}$ kg/ms. Fluidization velocities were 3 m/s and 0.4 m/s, respectively. Since the material properties and the fluid-dynamic conditions of the two test cases fall in the middle of the range of conditions in the simulations used for the estimation of the parameters, these two simulations represent a test of the interpolation capabilities of the correlations.

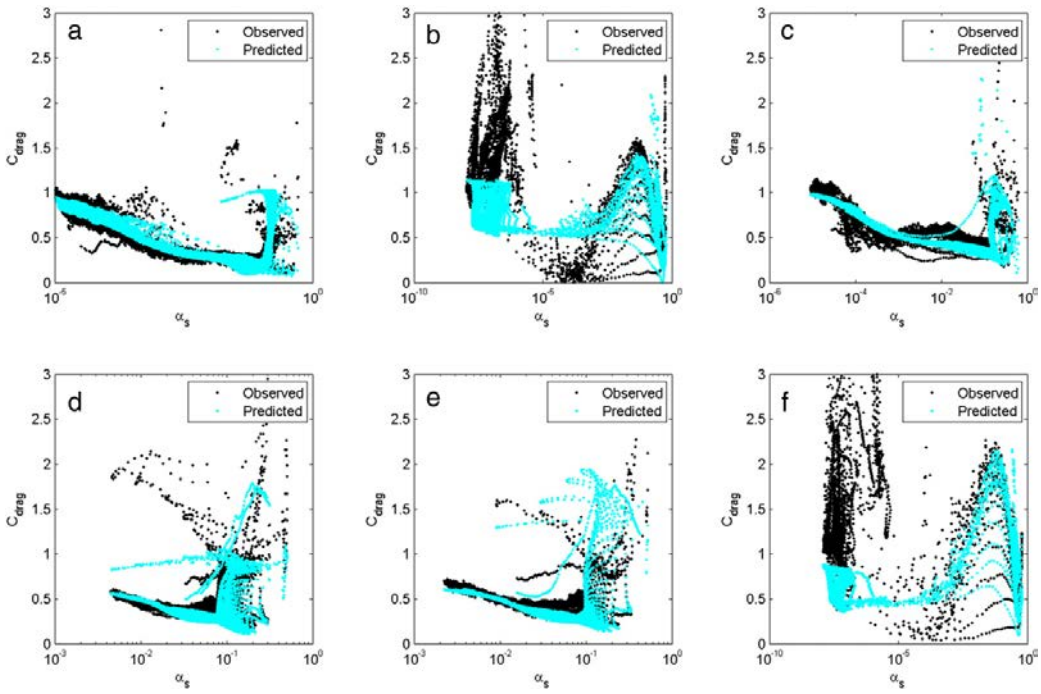


**Fig. 16.** Results obtained with a model that by means of blending functions combines the correlation for dilute CFB conditions with the general model, which is used for the bottom bed and dense conditions. Cases 19 (a), 59 (b), 63 (c), 6 (d), 29 (e) and 53 (f).

Fig. 19 shows a comparison between the observed and predicted $C_{drag}$ values. Data corresponding to the air distributor region (height below 0.1 m), walls (distance from the wall less than 0.02 m), exit region (distance to the exit less than 0.5 m) and the return channel were omitted from the comparison. The freeboard region in the BFB case was also removed from the figure. The results show a good match between the observed and the predicted values, at least qualitatively. Also quantitatively the results are satisfactory, with $R = 0.84$ for the CFB case and $R = 0.96$ for the BFB case, respectively, calculated for the data points shown in Fig. 19. Thus the correlation between observed and predicted values is practically as good as what was obtained for the cases that were included in the data set used for the parameter estimation. This indicates that the correlation is robust and safe to be used for simulations in the material property and fluid-dynamic ranges included in Table 1. An extrapolation to conditions outside the range covered in this work is risky. Due to the characteristics of the logistic sigmoid function, nonlinear empirical models based on logistic sigmoids have a potential of producing steep gradients outside the range for which they are derived. Thus the behavior of the function should be carefully evaluated before using it for extrapolation outside the range from which it was derived. A safer alternative would be to carry out a small number of transient simulations in the conditions where a correlation for $C_{drag}$ is needed and to include the new data in the data set to re-fit the model parameters.

## 5. Discussion

The results of the present study show that a fairly complicated drag correction function is required if the whole range from bubbling and turbulent beds to circulating fluidized beds has to be covered with a single correlation. In the present study, data from the wall and air distributor regions were omitted from the analysis. They could probably have been included in the same correlation, since the correlations developed from the reduced data set seem to be at least qualitatively capable of extrapolating to these regions. However, the flow patterns near the walls and above the air distributor are very different from the rest of the flow domain and widening the scope of a single correlation could require a larger number of parameters. Thus, separate correlations would need to be developed for the vicinity of walls and the air distributor region. The analysis of effects of the different kinds of gas-flow inlet also showed that, in bubbling bed conditions, the air distributor design can affect the drag correction needed in the entire bed area. Thus it is

**Table 3**
Blending function used to combine the correlation developed in Section 4.4 (denoted by $f_1$) with the correlation developed in Section 4.5 (denoted by $f_2$) to produce a continuous function $f_0$.

| Range | Blending function |
|---|---|
| $\log \alpha_s > -1.3$ or $z < 1.3$ m | $f_0 = f_1$ |
| $\log \alpha_s < -1.8$ and $z > 1.8$ m | $f_0 = f_2$ |
| $-1.8 < \log \alpha_s < -1.3$ and $z > 1.8$ m | $f_0 = f_1 + \frac{f_2 - f_1}{0.5}(z - 1.3)$ |
| $\log \alpha_s < -1.8$ and $1.3\ \text{m} < z < 1.8$ m | $f_0 = f_2 + \frac{f_2 - f_1}{0.5}(\log \alpha_s + 1.8)$ |
| $-1.8 < \log \alpha_s < -1.3$ and $1.3\ \text{m} < z < 1.8$ m | $f_0 = 4(f_1((1.8 - x)(-1.3 - \log \alpha_s) + (1.8 - z)(\log \alpha_s + 1.8) + (z - 1.3)(\log \alpha_s + 1.8)) + f_2(z - 1.3)(-1.3 - \log \alpha_s))$ |

Elevation $z$ in the blending function is given in meters.

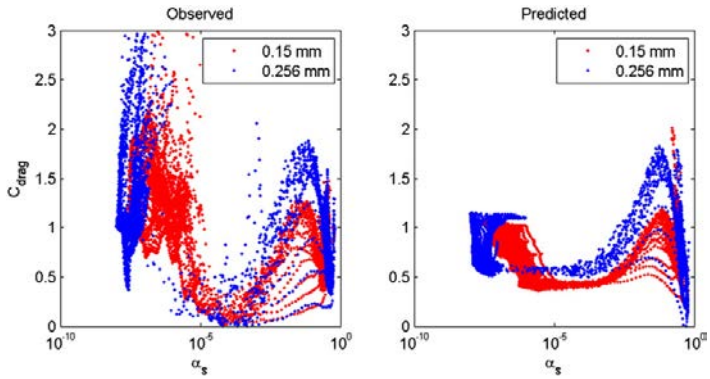


**Fig. 17.** Comparison of observed values and results obtained with a model that by means of blending functions combines the correlation for dilute CFB conditions with the more general model in two BFB cases with different particle sizes. Cases 57 and 58 in Table 2.

possible that a case-by-case consideration is required when choosing an appropriate correlation for different air distributor designs if high accuracy is desired.

The correlations developed in the present work are not necessarily the absolute best ones that could be developed on the basis of the data and the selected input variables. There are several possibilities to further improve the correlations. So far, only few possible configurations based on Eqs. (2)–(4) were tested. A bigger data set characterized by larger variations in the material properties would be necessary to fully take into account the possible combined effects of the different variables. This would make it possible to introduce a larger number of sigmoid functions in the correlation without reducing the correlation's robustness and interpolation capabilities.

The results also indicate that $C_{drag}$ behaves in a clearly different way in BFB and TFB conditions. If a simulation is limited to BFB conditions, a separate correlation would most likely work better than the more general correlation developed in the present study. It is likely that a more complicated correlation with even more parameters and a larger amount of simulation data would be needed for TFB conditions. However, since a large number of parameters leads to longer computations, an efficient approach would be to have separate correlations for different purposes and different regions, like those we developed here for the dilute CFB conditions, and to combine them to a unified model with blending functions.

In some cases it could also be beneficial to use a simpler correlation with fewer parameters that could be calibrated separately for each application. For such purpose, a large set of available transient simulation data could be collected and for each application the available data closest to the actual conditions could be used to update the model parameters. This could be useful in some conditions to improve the accuracy, especially for modeling cases with constant material properties. However, in industrial processes the conditions vary and e.g. at air inlets of a CFB combustor, the gas temperature can be below 100 °C while the typical temperatures in the furnace are in the range 750 °C–950 °C. In BFB combustion the temperature variations inside the furnace are even larger. The average particle diameter at the riser bottom in a CFB combustor is typically of the order of 0.4–1 mm whereas in the upper part of the riser, the average particle size is usually in the range of 0.1–0.2 mm. Thus in fluidized bed combustors, the range of temperatures and particle sizes vary in the full range covered in the present study rendering simplification of the correlation difficult.

There is also no guarantee that the chosen set of input variables is the optimal one. Furthermore, it should be noted that the empirical approach applied in this work produces correlations instead of models since a causal relation between the different input variables and the drag correction does not necessarily exist and it is in any case not easy to prove. Thus the current work simply looks for correlations between a set of input variables and $C_{drag}$. When one process variable in a fluidized bed is changed, the fluidization state can considerably change which complicates the analysis of causes and effects. There could be parameters, such as e.g. the stress components and the solid acceleration rate, that allow to better describe the local conditions. Since these parameters would complicate the evaluation of $C_{drag}$ during a steady state simulation they have not been accounted for at this stage.

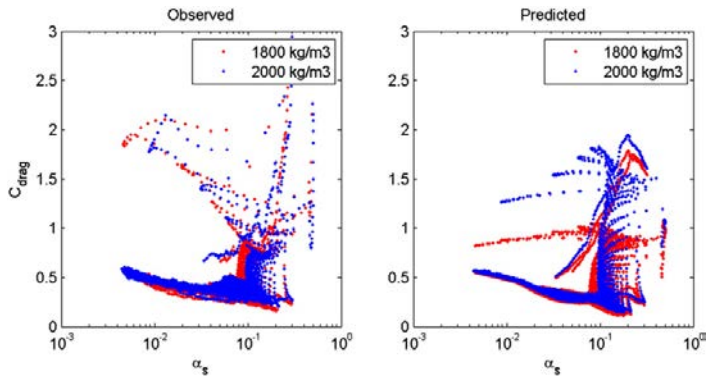


**Fig. 18.** Comparison of observed values and results obtained with a model that by means of blending functions combines the correlation for dilute CFB conditions with the general model in two CFB cases with different solid densities. Cases 6 and 5 in Table 2.

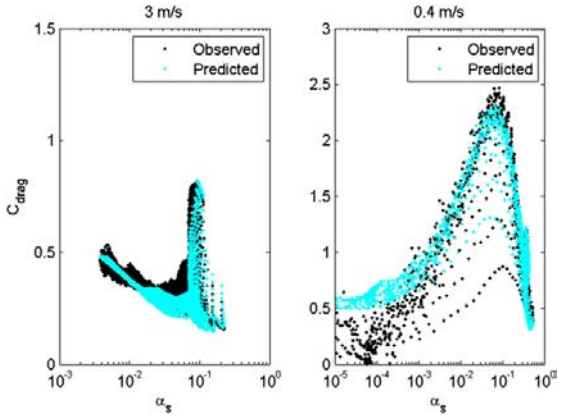


**Fig. 19.** A comparison between observed and predicted $C_{drag}$ values in a CFB (left) and a BFB (right) at conditions that were not included in the data set used for derivation of the correlation for $C_{drag}$.

Furthermore, other important variables, like particle size distribution [25] and shape [26], which are known to have significant effects on the drag force, were also omitted from this study. At present, no data of adequate quality are available to include these variables in the correlations, but the effects of these variables should be considered in the future.

The largest uncertainty in the correlations developed here comes from the 2D simplification of the transient simulations, which compromises the accuracy of the correlations when they are applied in 3D simulations. Still, in the absence of a more reliable model, the correlations developed in this work could also be used in 3D simulations as an approximation for the gas–solid drag force. It is also possible that in TFB simulations the results suffer from the 2D simplification even more than CFB simulations because of the more significant down flow of solids in the middle portion of a TFB. In a 3D geometry, the falling clusters have more freedom to avoid collisions with rising clusters than in 2D, which renders 2D simulations inadequate for TFB studies. Thus further 2D studies of the drag correction required for TFB conditions may not be worthwhile.

Before the correlations developed in this work can be implemented in a CFD code, steps should be taken to improve their computational performance. The correlations developed here contain a large number of model parameters. Many of them may be unnecessary and a superfluous burden for the computations, but no effort has been made here to check their role in the correlation. Such an investigation should be carried out before implementation. Furthermore the correlation showed behaviors that could be problematic during numerical simulations. The correlations occasionally predicted very small and even negative values and, especially close to the air distributor, excessively high values. Hence upper and lower limits, preferably case specific, should be set for $C_{drag}$ to avoid numerical complications. Most of the transient simulations in CFB conditions were carried out at high gas velocities which transported significant amounts of solids to the upper part of the riser. Thus the lowest solid concentrations in most of the CFD cases were far from zero, typically in the range 0.001–0.01. For example in circulating fluidized bed boilers, the local solid volume fraction in the upper part of the riser can be orders of magnitude lower. Thus the correlations need to be extended to lower solid concentrations, which can be done in the future by including more data from dilute conditions in the data set used as the basis for model development. By definition, $C_{drag}$ should be equal to unity in the homogeneous flow conditions at very low solid concentrations and at the packing limit. The present correlations fail to correctly reproduce these limits and thus need to be modified prior to implementation in a CFD code.

In the present study, the goal was to develop a correlation for the steady-state drag force between gas and solids in a multiphase flow. In the literature, a more common approach has been to develop subgrid closures for the drag force to be used in transient CFB simulations with limited spatial resolution [27,28,29,30]. These two topics are closely related since in both the effects of the inhomogeneity of the suspension are addressed. The only difference is the choice of the temporal and spatial scales for the filtering process. In the special case where the scale of the spatial filter is larger than the transient flow structures the subgrid scale closures are identical to the steady-state closures. Thus the obtained values of the correction function and the conclusions of the present study are also indicative for sub-grid modeling, but without the added complexity of accounting for the local spatial resolution of the simulation.

## 6. Conclusions

The present study evaluated possible approaches to cover all fluidization states by a single drag law in steady state CFD modeling. The time-averaged drag force was expressed as a product of the drag force calculated from the traditional drag laws for homogeneous conditions and a correction function. In Kallio et al. [10], parameters that could have significant effects on the correction function in CFB conditions were identified. They were the solid volume fraction, the distance from the nearest wall, the slip velocity between the phases, the particle size, the solid density and the gas viscosity. In the present paper, the analysis is extended to TFB and BFB conditions. A larger amount of data with wider variation in material properties was collected for evaluation of the possibilities to develop an empirical drag correction function by nonlinear regression analysis of data from transient simulations.

The work showed that covering all fluidized bed conditions in a single-drag correlation is feasible. To develop an acceptable correlation that behaves well in the bed region of a BFB, two additional input variables had to be taken into account, i.e. gas velocity and the elevation above the air distributor. However, no solution was found allowing a good description of the surface and freeboard regions of a bubbling bed with a correlation that would also be applicable in CFB conditions. A more complicated correlation would be necessary to simultaneously cover the dilute conditions in the upper part of a CFB riser and in the freeboard of a BFB. Such a correlation was considered too complicated. A more reasonable approach would be to divide the correlations into separate correlations for each different region that could be combined into a single correlation by means of blending functions. This approach was demonstrated by developing a separate correlation for the dilute conditions above 1.5-m height in CFB risers. The accuracy of the correlation improved significantly in dilute CFB conditions where a much simpler correlation with six input variables could be used.

In the present work, data from 69 transient CFD simulations were used as the basis for empirical modeling. In order to derive a more accurate correlation, a larger data set would be required, especially for the evaluation of the combined effects of the material properties. The largest uncertainty in the correlations here presented arises from the 2D simplification applied in the transient simulations. In many cases, 2D simulation results significantly differ from the 3D results, which compromises the accuracy of the correlations developed from 2D data when they are applied in 3D simulations. In the absence of a more reliable model, the correlations developed in this work could be used also in 3D simulations as an approximation for the gas–solid drag force. However, before implementing the correlations in CFD software, the correlations still require refinements to reduce the possibility of numerical complications and to improve the performance in conditions outside of the data range from which the correlations have been obtained. Because of these reservations, the correlation parameters were not given in the paper and the developed correlations should only be considered as a proof of the concept. So far, no models have been presented in the literature that would cover a wide range of fluidization

conditions. Thus, besides the approximations and limitations, the modeling approach presented in this paper can serve as a promising starting point for the development of a general drag law for CFD simulation of fluidized beds.

*Notation*

| | |
|---|---|
| $a$ | parameter |
| $b$ | parameter |
| $C$ | correction function |
| $d$ | diameter |
| $E$ | error sum |
| $e_{ss}$ | restitution coefficient |
| $g$ | gravitational acceleration $g_{0,ss}$ radial distribution function |
| $h$ | height |
| $\boldsymbol{I}$ | unit matrix |
| $I_{2D}$ | second invariant of the deviatoric stress tensor |
| $k_{\Theta_s}$ | diffusion coefficient of granular energy |
| $k$ | index |
| $K_{gs}$ | inter-phase momentum transfer coefficient |
| $N$ | number of |
| $p$ | pressure |
| $R$ | correlation coefficient |
| $Re$ | Reynolds number |
| $u$ | velocity |
| $U$ | time-averaged velocity |
| $U_0$ | superficial velocity |
| $v_t$ | terminal velocity |
| $w$ | riser width |
| $x$ | input variable |
| $\Delta x_{mesh}$ | mesh spacing |
| $\Delta x_{wall}$ | distance to the wall |
| z | value given by a sigma function |

*Greek symbols*

| | |
|---|---|
| $\alpha$ | volume fraction |
| $\phi_{gs}$ | energy exchange between gas and solids |
| $\eta$ | auxiliary variable |
| $\lambda_s$ | granular bulk viscosity |
| $\mu$ | viscosity |
| $\rho$ | density |
| $\tau$ | stress $\Theta_s$ granular temperature |
| $\gamma_{\Theta_s}$ | collisional dissipation of energy |

*Subscripts*

| | |
|---|---|
| col | collisional |
| drag | related to the drag force |
| fr | frictional |
| g | gas |
| kin | kinetic |
| max | maximum |
| obs | observed |
| $p$ | particle |
| pred | predicted |
| $s$ | solid |
| $t$ | related to the terminal velocity |
| $y$ | vertical coordinate direction |

*Superscripts*

| | |
|---|---|
| * | calculated from time-averaged values |

## Acknowledgment

The authors gratefully acknowledge the financial support of Tekes, VTT Technical Research Centre of Finland, Etelä-Savon Energia Oy, Fortum, Metso Power Oy and Numerola Oy, and the support from Saarijärven Kaukolämpö Oy.

## References

[1] V. Taivassalo, S. Kallio, J. Peltola, On time-averaged CFD modeling of circulating fluidized beds, Int. J. Nonlinear Sci. Numer. Simul. 13 (2012) 363–373.
[2] T.J. O'Brien, A multiphase turbulence theory for gas-solid flows: I. Continuity and momentum equations with Favre-averaging, http://dx.doi.org/10.1016/j.powtec.2014.01.030 .
[3] S. Kallio, V. Taivassalo, T. Hyppänen, Towards time-averaged CFD modelling of circulating fluidized beds, 9th Int. Conf. on Circulating Fluidized Beds, Hamburg, 2008.
[4] J. De Wilde, The generalized added mass revised, Phys. Fluids 19 (2007) 058103.
[5] J. De Wilde, G.J. Heynderickx, G.B. Martin, Filtered gas–solid momentum transfer models and their application to 3D steady-state riser simulations, Chem. Eng. Sci. 62 (2007) 5451–5457.
[6] S. Kallio, V. Poikolainen, T. Hyppänen, Mathematical modeling of multiphase flow in a circulating fluidized bed, Report 96–4, Heat Eng. Lab, Åbo akademi University, Turku, Finland, 1996.
[7] J.M. Matsen, Mechanisms of choking and entrainment, Powder Technol. 32 (1982) 21–33.
[8] C. Wen, Y. Yu, Mechanics of fluidization, Chem. Eng. Prog. Symp. Ser. 62 (1966) 100–111.
[9] D. Gidaspow, Multiphase flow and fluidization—continuum and kinetic theory descriptions, Academic Press, 1994.
[10] S. Kallio, J. Peltola, T. Niemi, Parametric study of the time-averaged gas–solids drag force in circulating fluidized bed conditions, accepted for publication, Powder Technol. 257 (2014) 20–29.
[11] D. Geldart, Types of gas fluidization, Powder Technol. 7 (1973) 285–292.
[12] T. Li, A. Gel, S. Pennala, M. Shahnam, M. Syamlal, CFD simulations of circulating fluidized bed risers, part i: grid study, Powder Technol. 254 (2014) 170–180.
[13] ANSYS Inc., ANSYS FLUENT Theory Guide. Release 14.0, Canonsburg, 2011. (2011).
[14] M. Syamlal, W. Rogers, T.J. O'Brien, MFIX documentation, Theory Guide, vol. 1, National Technical Information Service, Springfield, VA, 1993, (DOE/METC-9411004, NTIS/DE9400087).
[15] C.K.K. Lun, S.B. Savage, D.J. Jeffrey, N. Chepurniy, Kinetic theories for granular flow: inelastic particles in couette flow and slightly inelastic particles in a general flow field, J. Fluid Mech. 140 (1984) 223–256.
[16] D.G. Schaeffer, Instability in the evolution equations describing incompressible granular flow, J. Differ. Equ. 66 (1987) 19–50.
[17] S. Ogawa, A. Umemura, N. Oshima, On the equations of fully fluidized granular materials, J. Appl. Math. Phys. (ZAMP) 31 (1980) 483–493.
[18] S. Ergun, Fluid flow through packed columns, Chemical engineering progress 48 (1952) 89.
[19] S. Kallio, M. Guldén, A. Hermanson, Experimental study and CFD simulation of a 2D circulating fluidized bed, The 20th Int. Conf. on Fluidized bed combustion. May 18–20, Xi'an, China, 2009.
[20] D. Kunii, O. Levenspiel, Fluidization engineering, Butterworth-Heinemann, 1991.
[21] T. Niemi, W. Rogers, S. Kallio, Time averaged modeling of BFBs: Analysis of the terms in the momentum equations, Proceedings Fluidization XIV Conference, May 2013, Noordwijkerhout, The Netherlands, 2013, pp. 559–566.
[22] J. Leboreiro, G.G. Joseph, C.M. Hrenya, Revisiting the standard drag law for bubbling, gas-fluidized beds, Powder Technol. 183 (2008) 385–400.
[23] K. Hornik, M. Stinchcombe, H. White, Multilayer feed-forward networks are universal approximators, Neural Netw. 2 (1989) 359–366.
[24] D.W. Marquardt, An algorithm for least-squares estimation of nonlinear parameters, J. Soc. Ind. Appl. Math. 11 (1963) 431–441.
[25] R. Beetstra, M.A. van der Hoef, J.A.M. Kuipers, Drag force of intermediate Reynolds number flow past mono- and bidisperse arrays of spheres, AIChE J 53 (2) (2007) 489–501.
[26] A. Haider, O. Levenspiel, Drag coefficient and terminal velocity of spherical and nonspherical particles, Powder Technol. 58 (1989) 63–70.
[27] Y. Igci, S. Sundaresan, Verification of filtered two-fluid models for gas–particle flows in risers, AIChE J 57 (2011) (2011) 2691–2707.
[28] Y. Igci, S. Pannala, S. Benyahia, S. Sundaresan, Validation studies on filtered model equations for gas–particle flows in risers, Ind. Eng. Chem. Res. 51 (2012) 2094–2103.
[29] C.C. Milioli, F.E. Milioli, W. Holloway, K. Agrawal, S. Sundaresan, Filtered two-fluid models of fluidized gas-particle flows: new constitutive equations, 59 (2013) 3265–3275.
[30] S. Shah, J. Ritvanen, T. Hyppänen, S. Kallio, Wall effects on space averaged two-fluid model equations for simulations of gas–solid flows in risers, Chem. Eng. Sci. 89 (2013) 206–215.